Photocatalytic and sonocatalytic dye degradation by sulfur vacancy rich ZnS nanopowder

**Shrabani Ghosh · Madhupriya Samanta ·
Dipayan Sen · Samrat Sarkar · Sourav Sarkar ·
K. K. Chattopadhyay**

Abstract Photocatalytic dye degradation is one of the simple and convenient ways to eliminate effluents produced by paper, plastic, printing, and textile industries. ZnS is one of the most investigated catalysts on which different modifications are applied. Here, PVP-assisted zinc sulfide (ZnS) nanopowder is prepared hydrothermally. The photoluminescence spectra signify the generated intermediate state which is attributed to sulfur (S) vacancy as obtained from the theoretical analysis. This defect-induced ZnS has shown excellent Rhodamine B (RhB) dye degradation of 95% in 100 min with dye sensitization effect under UV irradiation. Under visible light, the degradation of RhB is only 50% in the presence of ZnS. The sensitization of RhB in the presence of UV light signifies the generation of visible light through the intermediate states caused by S vacancy. However, to eliminate the disadvantage of photocatalysis in highly concentrated wastewater management and expense of UV source, RhB is degraded by sonocatalysis, and 70% of dye is removed within 100 min in the presence of ZnS nanopowder. Therefore, the efficient catalytic dye degradations are achieved employing the minimum amount of ZnS powder.

Keywords ZnS · Photocatalysis · Sonocatalysis · Dye Sensitization · Sulfur vacancy · Nanostructures

S. Ghosh · M. Samanta · S. Sarkar · S. Sarkar ·
K. K. Chattopadhyay (✉)
School of Materials Science and Nanotechnology,
Jadavpur University, Kolkata 700032, India
e-mail: kalyan_chattopadhyay@yahoo.com

M. Samanta
Department of Electronics and Telecommunication
Engineering, Jadavpur University, Kolkata 700032, India

D. Sen
Department of Physics, Calcutta University,
Kolkata 700009, India

K. K. Chattopadhyay
Thin Film and Nano Science Laboratory, Department
of Physics, Jadavpur University, Kolkata 700032, India

Introduction

Since the last decade, environmental pollution is keeping a potentially harmful impact on human life as well as wildlife (Gupta 2009). The textile and allied industries release environmentally harmful effluents which pollute water acutely (Sharma et al. 2012). It has an adverse effect not only on the human being but also on the animal planet. The organic dyes which are not biodegradable are one of the major residues (Rai et al. 2005). Hence, organic dye degradation is one of the important fields of research, nowadays. Different conventional methods for dye removals such as precipitation, liquid–liquid extraction, filtration, and precipitations are limited by their own constraints (Sharma et al. 2012; Miretzky and Cirelli 2009; Huang et al. 2015; Hameed et al. 2007). Heterogeneous photocatalytic dye degradation is one

of the modern and convenient ways to eliminate the pollutants from aqueous and gaseous medium (Vieira et al. 2020; Zhang et al. 2021). In this field, the wide bandgap semiconductors have attracted the attention of the researcher due to its interesting optical properties (Ghosh et al. 2017). In this perspective, few oxide materials, such as TiO_2 and ZnO, are conventional wide bandgap semiconductors since the discovery of photocatalytic dye degradation process (Lakshmi et al. 1995; Sakthivel et al. 2003). Usually, they get activated by the light having UV wavelength. There have been numerous reports on the designing of semiconductor catalysts which get excited under visible light by creating defect states, doping, and composite or hybrid formation (Wu et al. 2020a, 2018, 2020b).

Zinc sulfide is a well-known n-type II-VI wide bandgap semiconductor in the field of photocatalysis since it can generate electron–hole pairs under UV photoexcitation (Lee and Wu 2017). It is one of the most popular photocatalysts for its substantially negative potential for excited electrons, low toxicity, and rapid generation of charge carriers (Fang et al. 2015). Apart from this, the intrinsic material properties like defect states, crystalline phases, and exposed facets are important factors to analyze the contribution of the catalyst in dye degradation (Fang et al. 2015; Wang et al. 2015; Kong et al. 2011; Pei et al. 2013; Zhang et al. 2008a). These factors can enhance the photocatlytic activity by the light-harvesting process (Zhang et al. 2008b). In addition, it can produce new adsorption sites preventing recombination of electron–hole pairs. However, optimum level of defects is beneficial because excessive defects can cause high rate of recombination degrading the photocatalytic activity (Wang et al. 2012; Lv et al. 2013). In the photocatalytic dye degradation process, vacancy defect modifies the electronic structure creating a new energy level in the forbidden region, which influences the properties of photo-generated charge carriers. ZnS is extensively studied including its Zn and S vacancy which have high impact on photocatalysis. S vacancies can cause the decrement of bandgap, whereas Zn vacancy leads to enlargement of bandgap (Chen et al. 2010; McCloy et al. 2013). Gang Wang reported controlled sulfur vacancy in the ZnS sphere which influenced the photocatalytic H_2 evolution under visible light (Wang et al. 2015). Hao et al. reported intrinsically Zn-deficient ZnS which

had shown enhanced photocatalytic H_2 evolution under visible light irradiation (Hao et al. 2018). Intrinsically created sulfur vacancy and wurtzite-sphalerite phase junction in ZnS instigated the visible light activated H_2 evolution as reported by Zhibin Fang (Fang et al. 2015). Fran Kurnia introduced defects in the forbidden region of ZnS nanoparticles in a controlled manner by which visible light absorption was achieved (Kurnia et al. 2016). T. Mahvelati-Shamsabadi et al. produced defect-induced ZnS by ultrasonication, and it showed outstanding performance in dye degradation under UV and sunlight irradiation (Mahvelati-Shamsabadi and Goharshadi 2017). Jaewon Lee prepared S vacancy controlled, porous, and hollow nanoplates of ZnS which had improved the UV-assisted photocatalytic activity than commercial material (Lee et al. 2018).

In UV-assisted photocatalytic dye degradation process, UV source is the major limitation for practical implementation due to its high cost and harmful effect. Apart from this, photocatalysis itself has a drawback of light penetration through highly concentrated and non-transparent dye wastewater (Farhadi and Siadatnasab 2016). Therefore, there are requirements to welcome new and innovative technologies and catalysts for highly concentrated dye removal. In this perspective, semiconductor-assisted sonocatalytic dye degradation can eliminate the drawback of photocatalysis by its strong penetration capacity through any water medium (Min et al. 2012). The process is based on hotspot theory and sonoluminescence (Zhou et al. 2015; Khataee et al. 2018).

In this work, PVP-capped ZnS is synthesized hydrothermally. It contains sulfur vacancy intrinsically as obtained from PL spectra and theoretical analysis. Although such vacancy is not able to activate ZnS under visible light spectra, a different UV light-assisted photocatalytic RhB degradation is observed with low concentration of ZnS. Besides, there is a limitation in practical implementation of expensive and harmful UV sources of light. There are different ways to eliminate the UV photocatalysis. One process is to modify the catalyst, and another is to apply different catalytic processes. In addition, it is difficult to degrade highly concentrated wastewater by photocatalysis process. Here, simple sonocatalytic dye degradation is performed in presence of ZnS. It also exhibits impressive catalytic dye degradation within 100 min as a first time report.

Experimental

Synthesis

All the reagents are of analytical grade and used without further purification. In this synthesis, 4 mmol zinc acetate dihydrate $(Zn(CH_3COO)_2,2H_2O)$ and 6 mmol of thiourea are dissolved in 80 mL of ethylene glycol, and 0.320 g of polyvinyl pyrrolidone (PVP) is added into the solution. After stirring for 30 min, the final precursor solution is transferred into a 100 mL Teflon lined stainless steel autoclave. The system is put in a preheated oven at 180°C for 24 h. The precipitates are centrifuged with deionized water and ethanol alternately. Then, the last contains are dried in a vacuum oven.

Computational details

Our density functional theory-based first-principles calculations are carried out using CASTEP code (Segall et al. 2002) which implements a supercell approach to density functional theory. Generalized gradient approximation, namely the Perdew Burke Ernzerhof (PBE) functional (Perdew et al. 1996), is used to describe the exchange and correlation terms. Vanderbilt ultrasoft pseudo-potentials (Vanderbilt 1990) are used to represent the ion cores of zinc, cadmium, and sulfur atoms, and plane waves up to energy cut off 290 eV are considered in the calculations. Brillouin zone integrations are carried out within the Monkhorst–Pack scheme (Monkhorst and Pack 1976) using a k-point mesh having effective separation of 0.071/Å in all directions. For geometrical optimization, both the atoms and cell dimensions are allowed to fully relax using BFGS (Broyden-Fletcher-Goldfarb-Shanno) scheme (Pfrommer et al. 1997) until the total energy converged to less than 2×10^{-5} eV/atom, the maximum force converged to lower than 0.05 eV/Å, and the maximum displacement is 0.002 Å. All calculations are performed in spin unrestricted manner; however no spin polarization is observed in any of the considered models.

In the current work, a $2 \times 2 \times 2$ supercell of ZnS (F-43 M, IT#: 216) containing 32 Zn and 32 S atoms is used. Optimized lattice parameters of all considered systems are listed below in Table 1.

Table 1 lists the optimized lattice parameters as obtained from DFT analysis.

Catalytic dye degradation

Photocatalytic activity of ZnS is studied under visible and UV light irradiation in the laboratory set up. UV light source is the tube of 40 W with maximum emission of 256.4 nm. The visible light source is mercury lamp with the specification of HPL-N 400 W/542 E40 HG 1SL PHILIPS with luminous flux of 22,000 lm. Sonocatalytic dye degradation is investigated using probe sonicator (frequency = 20 kHz advanced probe sonicator PKS-750F with 13mm titanium probe, maximum output power = 750 W, 15% of maximum output amplitude is used) as a source of ultrasound by which RhB dye is degraded within 100 min.

Typically, 10 mg of ZnS is mixed in 60 mL of 10^{-5} mol L^{-1} RhB solution and stirred in the dark for 1 h to reach the adsorption–desorption equilibrium. Then, the system is placed under ultrasonic probe/visible/UV irradiation. For every experimental process, 5 mL of reaction solution is taken as specimen at regular time intervals, and then, it is centrifuged and filtered to get rid of the existing catalyst sample. The absorbance spectra of the collected specimens are examined by UV–Vis absorption spectroscopy. The experimental vessel is double walled with a continuous flow of cold water within the walls to sustain uniform temperature.

Degradation efficiency

The degradation efficiency is analyzed by C_t/C_0 vs. time plot, where C_0 is the initial concentration of dye and C_t is the concentration of dye at time t in the process of degradation. It also gives a perception about the percentage degradation of RhB dye in the presence of catalyst under ultrasound/visible/UV irradiation with respect to initial concentration of RhB. The equation is presented in Eq. (1) (Samanta et al. 2018).

Table 1 Optimized lattice parameters for ZnS

System	A (Å)	B (Å)	C (Å)
ZnS	10.916	10.916	10.916

$$Degradation\ (\%) = \frac{C_0 - C_t}{C_0} \times 100 \qquad (1)$$

Pseudo-first-order model

To define the reaction rate of catalytic dye degradation, a pseudo-first-order model is applied. As per condition, if C_0 is small enough, the reaction is called pseudo-first-order with a constant rate coefficient (Samanta et al. 2018):

$$ln\frac{C_0}{C_t} = k_{app}t$$

where k_{app} is the apparent reaction coefficient.

Characterizations

The as-synthesized ZnS is characterized by X-ray diffraction (XRD Bruker, D8 Advance) operating at 40 kV and 40 mA in the 2Θ range of 20°–80° for assuring its phase. The structural analysis of the sample is done by a field emission scanning electron microscope (FESEM, Hitachi, S-4800) operated at an accelerating voltage of 5 kV. High-resolution transmission electron microscopy is also carried out to understand its morphology and crystallinity (HRTEM, JEOL-JEM) more accurately. The bandgap from reflectance spectra and quantification of removal efficiency have been estimated by UV–Vis spectroscopy (Shimadzu, UV-3600). Photoluminescence study is performed using Edinburgh FLS980 PL spectrometer.

Results and discussion

The solvothermally synthesized white powder is characterized by XRD in Fig. 1a. It shows the prime XRD peak positions at 28.8º, 47.86º, and 56.66º, which completely agree with the JCPDS card number 06–0566. Therefore, it confirms the formation of the zinc blende phase of ZnS with high purity. In addition, there is a visible broadening in XRD peaks which indicates the formation of small crystallites in the particles. The detailed study is discussed in our previous reports (Ghosh et al. 2017).

The FESEM image of ZnS presented in Fig. 1b defines the agglomerated ZnS nanoparticles with diameters 80 to 120 nm. Since PVP acts as a capping agent, the structure of ZnS is not exactly spherical in nature. Furthermore, the structural analysis of ZnS is carried out using TEM, and it is displayed in Fig. 2a. It is reassuring about the formation of ZnS nanoparticles with diameter around 100 nm. Although exact spherical structure is not observed, ZnS comprises almost equal sized nearly spherical particles throughout the distribution. To reassure the observation, the histogram has been presented in the inset of Fig. 2a on the basis of TEM image of ZnS. It exhibits that the diameter of ZnS nanoparticles lies between 75 to 120 nm with the maximum number of nanoparticles containing the diameter of 100 ± 10 nm. It is depicted from the histogram that the mean diameter of ZnS nanoparticle is 100 nm with the standard deviation of 11 nm.

To determine the exact Zn to S ratio in the solvothermally synthesized ZnS nanopowder, the EDS analysis is carried out and shown in Fig. 2b–e. It is observed from Fig. 2b that there is no impurity in ZnS in the focused region. It is evident from the

**Fig. 1** (**a**) XRD pattern and (**b**) FESEM of solvothermally synthesized ZnS nanopowder
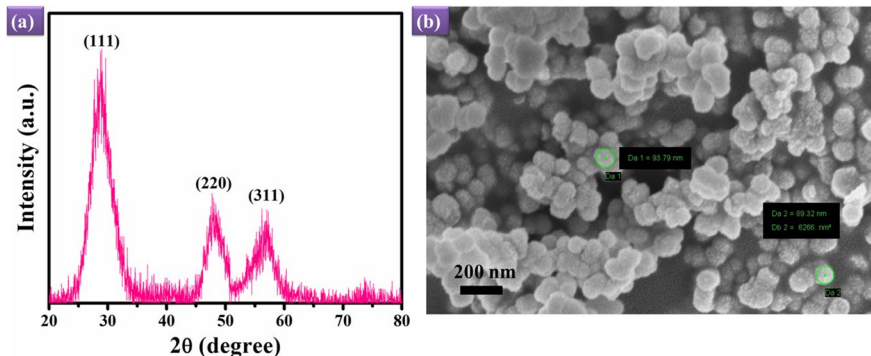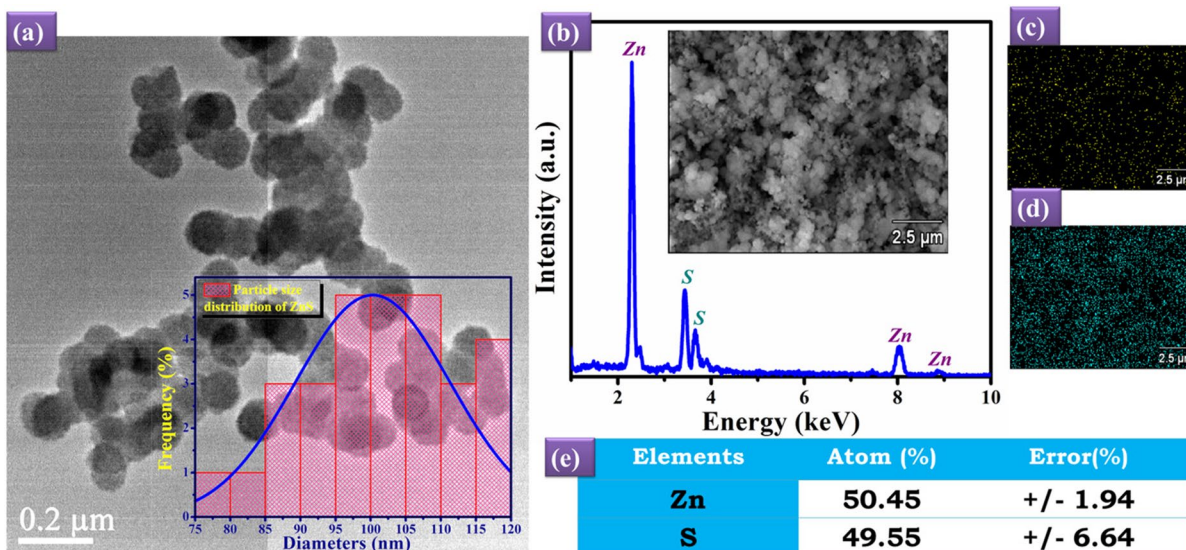
Fig. 2 (**a**) TEM with particle size distribution of ZnS, (**b**) EDS analysis, (**c**) Zn and (**d**) S mapping, (**e**) elemental distribution of ZnS nanopowder

spatial distribution of zinc and sulfur in Fig. 2c and d, respectively, that Zn and S are homogeneously spread throughout the region. Figure 2e confirms the actual stoichiometry of zinc and sulfur in ZnS in terms of atomic % which is almost 1:1 with an acceptable error bar.

To obtain the bandgap of ZnS, UV–Vis diffuse reflectance spectroscopy (DRS) is performed and shown in Fig. 3a. ZnS has high reflectivity of 80 to 95% in the visible region. There is a sharp fall of reflectance curve at 355 nm. The bandgap (E_g) is calculated to be 3.73 eV from Kubelka–Munk formula considering ZnS a direct bandgap semiconductor

(Lee and Wu 2017). Thus, such wide bandgap semiconductors can be activated by UV light irradiation only. The RAMAN spectra of ZnS show highly fluorescent property in Fig. 3b. Hence, no characteristic peak shifting is obtained.

To verify the photoluminescence (PL) property of ZnS (cf. Figure 3c), it is excited at 467 nm of wavelength equivalent to approximate energy of 2.65 eV. The excitation results in a broad and strong green emission at 524 nm equivalent to around 2.36 eV which was already presented in our previous report (Ghosh et al. 2017). It is actually defining the luminescence in the green region of visible
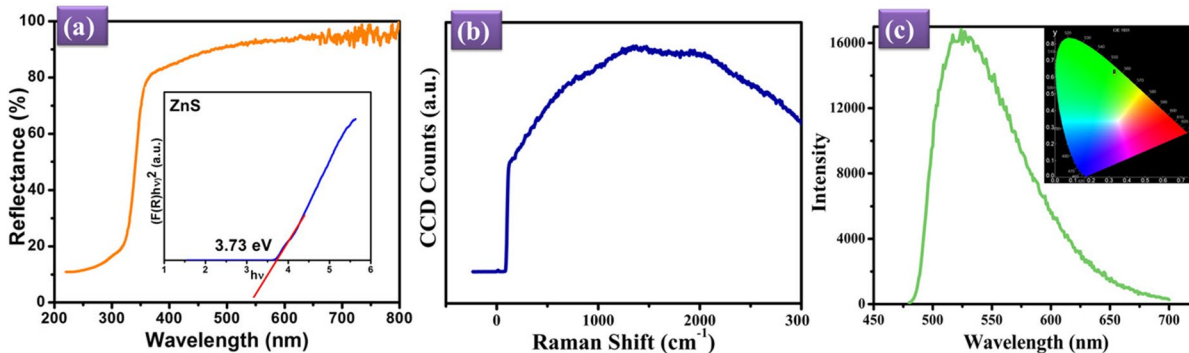

Fig. 3 (**a**) Reflectance, bandgap (inset), (**b**) RAMAN spectra, and (**c**) photoluminescence spectra of ZnS nanopowder

light wavelength as obtained from the chromaticity diagram. Therefore, since the exciting and emitting both energies are lower than the bandgap energy of 3.73 eV, the intermediate states situated in the forbidden region are responsible for the photoluminescence property. To analyze such phenomenon, a schematic has been represented in Fig. 4a. It illustrates that in the forbidden region, there are intermediate states near the conduction band edges. By excitation of 467 nm of light, the electron gets excited from valance band (VB) to the intermediate states situated at 2.65 eV from VB. Consecutively, by non-radiative intra-band transition, the electron positions at the intermediate state of 2.36 eV, and then, it transfers to the VB by radiative emission of 524 nm and recombines with the hole in VB. Thus, the electron transfer process can be proposed in PL. Generally, two types of emissions are observed during the room temperature PL in II-VI semiconducting materials. One is intrinsic near band edge emission for bandgap property, and another is extrinsic deep level emission due to the presence of defect or modification of electronic structure. Denzer et al. proposed that different lattice defects caused luminescence with broad spectrum in lower energy region compared to the bandgap energy (Denzler et al. 1998). Such defects include interstitials and vacancies of Zn and S in ZnS lattices. The vacancy and interstitial of Zn can act as localized acceptor and donor level, while the vacancy and interstitial of S can be treated as localized donor and acceptor states, respectively (Bhattacharjee and Lu 2006). Hence, it can be assumed that such interesting PL property is primarily due to the experimentally induced lattice defects in ZnS.

For the convenience of calculation, vacancy of Zn and S in ZnS has been taken under considered. To find out the source of intermediate states in the forbidden region, first-principles computations of density of states (DOS) are conducted for pure ZnS and defect-induced ZnS with sulfur and zinc vacancy. Figure 4b describes that pure ZnS and ZnS with Zn vacancy have almost similar TDOS (Total DOS) with the same position of conduction band minima and valence band maxima. Sulfur vacancy in ZnS causes generation of new states near conduction band edge. Therefore, from this theoretical point of view, it can be said that the intermediate defect states are induced due to the sulfur vacancy near the zinc atom in ZnS. To elucidate the exact contribution of the orbital, PDOS (projected density of states) is calculated for Zn near S vacancy of ZnS. It elaborates that 3s and 4p orbitals of Zn atom near sulfur vacancy have high impact in the formation of intermediate states, whereas d orbital has no participation in it (*cf.* Figure 4c).

To investigate the catalytic activity of synthesized ZnS nanopowder, the RhB organic dye is employed as pollutant in water, and 10 mg of ZnS is used as catalyst under different types of irradiations. At first, photocatalytic RhB dye degradation is performed under two different light illuminations: (1) visible range and (2) UV range light. Figure 5a shows the absorbance spectra of RhB in presence of ZnS under visible light irradiation. Here, after certain adsorption of RhB on the catalyst surface after 1 h of dark stirring, ZnS exhibits poor catalytic degradation even after 100 min of illumination. Besides, Fig. 5b explores the UV-illuminated photocatalysis and dye sensitization with
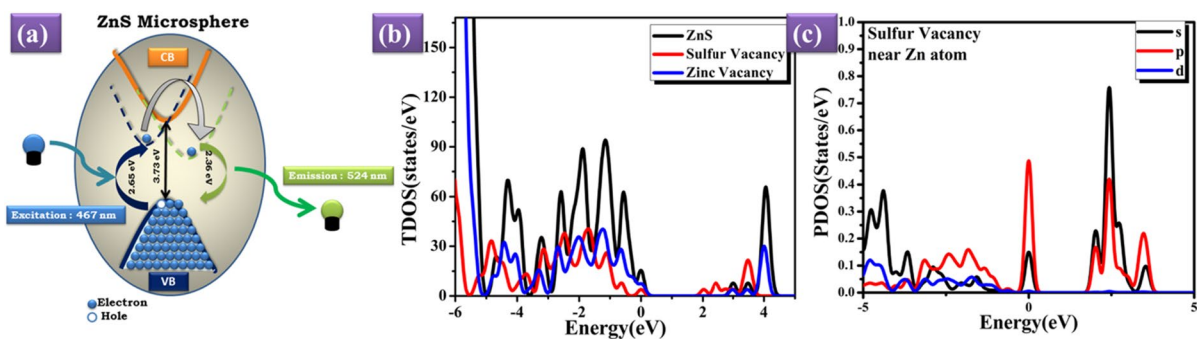
Fig. 4 (**a**) Schematic representation of PL from ZnS, (**b**) TDOS of ZnS, and sulfur, zinc vacancy contained ZnS (**c**) PDOS of sulfur vacancy near Zn atom in ZnS

Fig. 5 UV–Vis absorption spectra of RhB in different time intervals under (**a**) UV (**b**) visible light irradiation and (**c**) sonication employing ZnS as catalyst. (**d**) Degradation profile of RhB under different conditions in the presence of ZnS
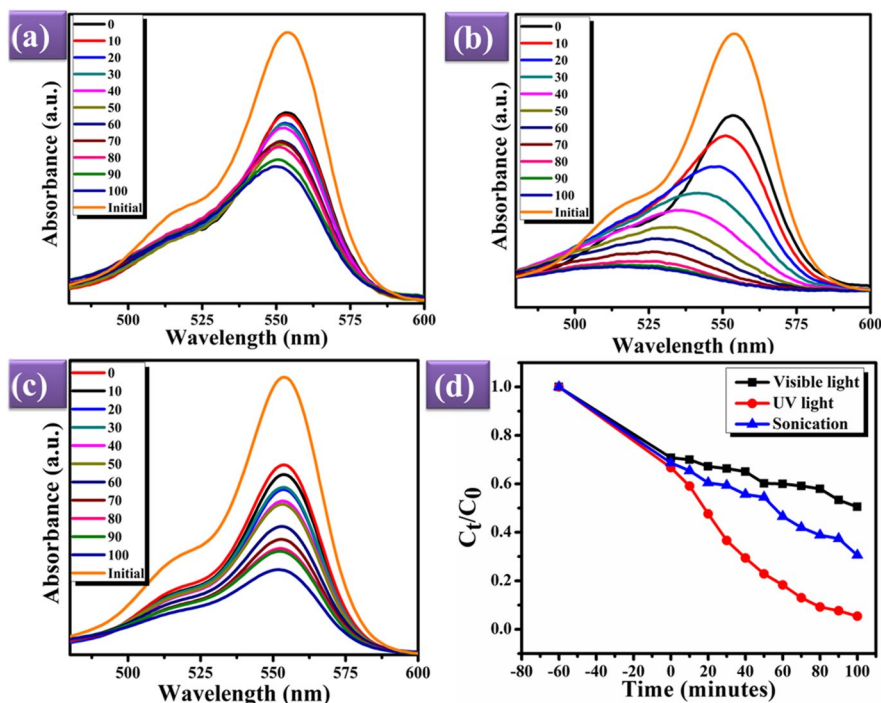

efficient dye removal ability of ZnS. Here, the degrading absorbance spectra and disappearance of characteristic peak of RhB after 100 min give the information about complete dye degradation under UV irradiation. There is a visible blue shift of absorbance spectra which may indicate N-de-ethylation of RhB (Barras et al. 2012; Wu et al. 1998). Since UV light source is highly expensive and harmful, ultrasound-assisted dye degradation is conducted here in the presence of ZnS as sonocatalyst, and corresponding absorbance spectra of RhB under ultrasound-assisted catalysis is presented in Fig. 5c. As it is observed that the absorbance peak of RhB is not totally disappeared even after 100 min of ultrasound irradiation, thus this pathway of catalysis in the presence of ZnS can be termed as moderate. It is not as efficient as UV light-assisted catalysis but also not as poor as visible light-driven photocatalysis. Additionally, it is environment-friendly and also cuts the expense of UV source as well as eliminates the necessity of any external light source. Moreover, it is efficient in the removal of highly concentrated organic dyes.

To investigate the rate of reaction in dye degradation under different conditions, degradation profile of RhB (C_t/C_0 vs. time) is plotted at different time intervals in Fig. 5d. It exhibits that ZnS achieves

adsorption–desorption equilibrium after 1 h of dark stirring and at $t = 0$ in Fig. 5d indicates the degradation of RhB in dark due to adsorption on the surface of ZnS. Here, C_t and C_0 are the concentration of dye at time t and $t = 0$, respectively. The highest rate of degradation is observed under UV light illumination in the presence of ZnS photocatalyst, and poor degradation of RhB is achieved under visible light keeping the rest conditions unchanged, whereas sonication gives moderate rate of reaction in the same scenario.

The degradation percentage of RhB with time is plotted in Fig. 6a under different sources of activation. It shows that almost 30% of RhB is degraded by the adsorption on the ZnS surface during dark stirring. Rest 70% of dye is removed by different catalytic activities of ZnS under different conditions. From the analysis, it can be understood that 95% of RhB is degraded under UV light irradiation in the presence of ZnS, whereas the degradation percentage is 50% under visible light and 70% under ultrasound sonication in the same environmental condition. It can be assumed that the photocatalytic activity of ZnS is almost static under visible light irradiation since the degradation is only 20% under illuminating conditions. It is even quite obvious due to the wide bandgap
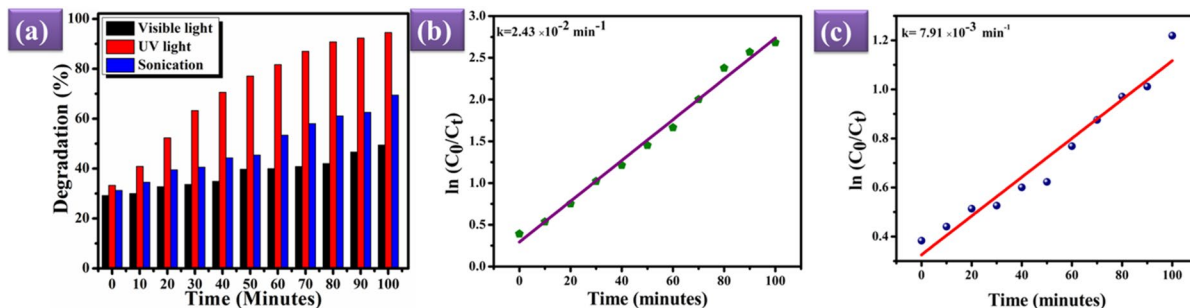
Fig. 6 (**a**) Degradation percentage of RhB with time in the presence of ZnS as catalyst, pseudo-first-order reaction kinetics for (**b**) UV light (**c**) ultrasound irradiation

nature of ZnS. The impressive UV light activated photocatalysis can be attributed to the wide band-gap of ZnS (Lee and Wu 2017; Fang et al. 2011) and dye sensitization which is also very rare under such conditions. Sonocatalysis pursues a completely different phenomenon which is able to activate ZnS in degrading the RhB dye. To investigate the reaction kinetics rate of RhB in the presence of ZnS under UV light and sonication, pseudo-first-order model is analyzed in Fig. 6b and c, respectively. The degradation rate of RhB (k) is 2.43×10^{-2} min^{-1} under UV radiation which is higher than $k = 7.91 \times 10^{-3}$ min^{-1} under ultrasound in presence of ZnS as catalyst.

Mechanism

UV-irradiated photocatalytic RhB degradation is the most efficient among all the above-mentioned procedures in the presence of ZnS. It is quite common and vastly reported that ZnS is ideal as a UV catalyst due to its wide bandgap nature which is true in this case also. In addition, hypochromic shift in absorbance spectra of RhB is observed under UV illumination which is not common. From the absorbance curve, it can be said that the degradation is not pure photocatalytic degradation, but there is a contribution of dye sensitization. RhB is well-reported to be sensitized under visible light, but the phenomenon is quite different here. To explain such a process, a schematic is proposed in Fig. 7 for elaborating the mechanism
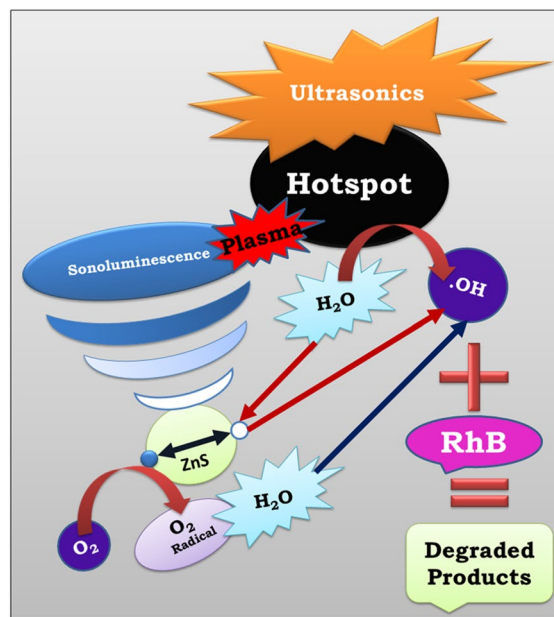
Fig. 7 Reaction mechanism of dye degradation under UV excitation in the presence of ZnS photocatalyst
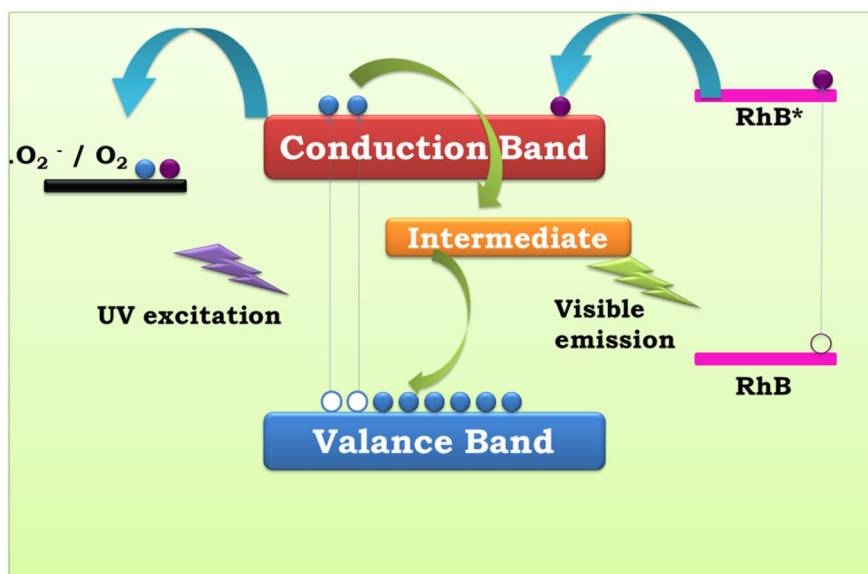
of RhB degradation using ZnS as photocatalyst. Figure 7 exhibits that ZnS gets excited by a UV light source creating electron–hole pair. It is already discussed that ZnS contains intermediate states which can act as trap states for excited electrons. After that, the electrons present in intermediate states recombine with the holes in the VB emitting visible light in the green wavelength which may excite the RhB to perform the N-de-ethylation by its own (Barras et al. 2012). The electrons excited in RhB due to intrinsic activation from catalyst are injected to the conduction band of ZnS. Then, RhB starts to be degraded by different ethylation reactions which are triethylrhodamine, die-thylrhodamine, ethylrhodamine, and rhodamine with different λ_{max} at 539 nm, 522 nm, 510 nm, and 498 nm, respectively (Barras et al. 2012; Wu et al. 1998; Akir et al. 2016). Thus, a visible shifting in absorbance spectra of RhB is observed even under UV illumination, and RhB gets mineralized. The excited electrons participate in a reaction with molecular oxygen by forming superoxide radicals which initiate the complete degradation of RhB. The generated holes produce hydroxyl ions reacting with water molecules and degrade the organic dye producing CO_2 and water.

When the material ZnS is concerned, the sonocatalytic dye removal is new to it. By ultrasonic irradiation, RhB is degraded using ZnS as sonocatalyst. There is a mechanism in Fig. 8 by which dye degradation phenomenon has occurred (Farhadi and Siadatnasab 2016; Min et al. 2012; Zhou et al. 2015). Generally, acoustic cavitation bubbles are formed under ultrasound, and they tend to be bigger attaining a critical size. After that, they start to collapse, and a high pressure is generated within the bubbles. By focusing toward the center of the bubbles, a shockwave directs and creates high pressure (1000 atm) and temperature (5000 K) at the core (Farhadi and Siadatnasab 2016; Zhou et al. 2015). This is called a hotspot which participates in the pyrolysis of water forming hydroxyl ions. In addition, the temperature generated in hotspot produces plasma when it collapses. It causes emission of light covering a wide spectral region. This phenomenon is termed as sonoluminescence which excites the electron of ZnS from valence band to conduction band and generated intermediate states. After that, the excited electrons react with oxygen resulting in superoxide radical which produces OH radicals. Additionally, the generated holes cause

Fig. 8 Reaction mechanism of dye degradation under ultrasound irradiation in the presence of ZnS sonocatalyst

the creation of ·OH. These radicals participate in the dye degradation procedure and transform the organic pollutant into CO_2 and water.

Conclusion

Hence, it can be concluded that sulfur vacant defect enriched zinc sulfide nanopowder is synthesized successfully via one-step solvothermal process. Though it is not an efficient photocatalyst in visible light due to its wide bandgap, it is a very efficient photocatalyst under UV light which is not only for its bandgap but also the generated intermediate states. It is proved that such defects are induced by sulfur vacancy in ZnS. These states participate in sensitization of RhB under UV illumination by generating visible range photoemission. As it is well-known that UV light is expensive and hazardous to human health, ultrasound-assisted catalysis is introduced using ZnS as a catalyst. Although the removal rate of toxicity is not as fast as UV, it is efficient enough in degradation of RhB. Above all, the experiments are conducted with very low concentration of samples such as 0.16 g/L. Therefore, it is advantageous to separate the catalyst

from the water. In future, the sonocatalytic activity of ZnS can be improved by developing new composites.

Declarations

Conflict of interest The authors declare no competing interests.

References

Akir S, Barras A, Coffinier Y, Bououdina M, Boukherroub R, Omrani AD (2016) Eco-friendly synthesis of ZnO nanoparticles with different morphologies and their visible light photocatalytic performance for the degradation of Rhodamine B. Ceram Int 42:10259–10265. https://doi.org/10.1016/j.ceramint.2016.03.153

Barras A, Cordier S, Boukherroub R (2012) Fast photocatalytic degradation of rhodamine B over [Mo6Br 8 (N3) 6] 2– cluster units under sun light irradiation. Appl Catal B 123:1–8. https://doi.org/10.1016/j.apcatb.2012.04.006

Bhattacharjee B, Lu CH (2006) Multicolor luminescence of undoped zinc sulfide nanocrystalline thin films at room temperature. Thin Solid Films 514:132–137. https://doi.org/10.1016/j.tsf.2006.02.096

Chen JH, Zeng XQ, Chen Y, Zhang HP (2010) First-principle theory calculations of electronic structure of sphalerite with vacancy and impurity. Chin J Nonferrous Met 20:765–771

Denzler D, Olschewski M, Sattler K (1998) Luminescence studies of localized gap states in colloidal ZnS nanocrystals. J Appl Phys 84:2841–2845. https://doi.org/10.1063/1.368425

Fang X, Zhai T, Gautam UK, Li L, Wu L, Bando Y, Golberg D (2011) ZnS nanostructures: from synthesis to applications. Progr Mater Sci 56(2):175–287. https://doi.org/10.1016/j.pmatsci.2010.10.001

Fang Z, Weng S, Ye X, Feng W, Zheng Z, Lu M, Liu P et al (2015) Defect engineering and phase junction architecture of wide-bandgap ZnS for conflicting visible light activity in photocatalytic H2 evolution. ACS Appl Mater Interfaces 7:13915–13924. https://doi.org/10.1021/acsami.5b02641

Farhadi S, Siadatnasab F (2016) Copper (I) sulfide (Cu2S) nanoparticles from Cu (II) diethyldithiocarbamate: synthesis, characterization and its application in ultrasound-assisted catalytic degradation of organic dye pollutants. Mater Res Bull 83:345–353. https://doi.org/10.1016/j.materresbull.2016.06.030

Ghosh S, Sarkar S, Das BK, Sen D, Samanta M, Chattopadhyay KK (2017) Band edge tuned Zn x Cd 1–x S solid solution nanopowders for efficient solar photocatalysis. Phys Chem Chem Phys 19:29998–30009. https://doi.org/10.1039/C7CP06305A

Gupta VK (2009) Application of low-cost adsorbents for dye removal–a review. J Environ Manage 90:2313–2342. https://doi.org/10.1016/j.jenvman.2008.11.017

Hameed BH, Din AM, Ahmad AL (2007) Adsorption of methylene blue onto bamboo-based activated carbon: kinetics and equilibrium studies. J Hazard Mater 141:819–825. https://doi.org/10.1016/j.jhazmat.2006.07.049

Hao X, Wang Y, Zhou J, Cui Z, Wang Y, Zou Z (2018) Zinc vacancy-promoted photocatalytic activity and photostability of ZnS for efficient visible-light-driven hydrogen evolution. Appl Catal B 221:302–311. https://doi.org/10.1016/j.apcatb.2017.09.006

Huang L, Luo F, Chen Z, Megharaj M, Naidu R (2015) Green synthesized conditions impacting on the reactivity of Fe NPs for the degradation of malachite green. Spectrochim Acta Part A Mol Biomol Spectrosc 137:154–159. https://doi.org/10.1016/j.saa.2014.08.116

Khataee A, Eghbali P, Irani-Nezhad MH, Hassani A (2018) Sonochemical synthesis of WS2 nanosheets and its application in sonocatalytic removal of organic dyes from water solution. Ultras on Sonochem 48:329–339. https://doi.org/10.1016/j.ultsonch.2018.06.003

Kong M, Li Y, Chen X, Tian T, Fang P, Zheng F, Zhao X (2011) Tuning the relative concentration ratio of bulk defects to surface defects in TiO2 nanocrystals leads to high photocatalytic efficiency. J Am Chem Soc 133:16414–16417. https://doi.org/10.1021/ja207826q

Kurnia F, Ng YH, Amal R, Valanoor N, Hart JN (2016) Defect engineering of ZnS thin films for photoelectrochemical water-splitting under visible light. Sol Energy Mater Sol Cells 153:179–185. https://doi.org/10.1016/j.solmat.2016.04.021

Lakshmi S, Renganathan R, Fujita S (1995) Study on TiO2-mediated photocatalytic degradation of methylene blue. J Photochem Photobiol A 88:163–167. https://doi.org/10.1016/1010-6030(94)04030-6

Lee GJ, Wu JJ (2017) Recent developments in ZnS photocatalysts from synthesis to photocatalytic applications—a review. Powder Technol 318:8–22. https://doi.org/10.1016/j.powtec.2017.05.022

Lee J, Ham S, Choi D, Jang DJ (2018) Facile fabrication of porous ZnS nanostructures with a controlled amount of S vacancies for enhanced photocatalytic performances. Nanoscale 10:14254–14263. https://doi.org/10.1039/C8NR02936A

Lv Y, Yao W, Ma X, Pan C, Zong R, Zhu Y (2013) The surface oxygen vacancy induced visible activity and enhanced UV activity of a ZnO 1–x photocatalyst. Catal Sci Technol 3:3136–3146. https://doi.org/10.1039/C3CY00369H

Mahvelati-Shamsabadi T, Goharshadi EK (2017) Photostability and visible-light-driven photoactivity enhancement of hierarchical ZnS nanoparticles: the role of embedment of stable defect sites on the catalyst surface with the assistant of ultrasonic waves. Ultrason Sonochem 34:78–89. https://doi.org/10.1016/j.ultsonch.2016.05.021

McCloy JS, Wolf W, Wimmer E, Zelinski BJ (2013) Impact of hydrogen and oxygen defects on the lattice parameter of chemical vapor deposited zinc sulfide. J Appl Phys 113:023706. https://doi.org/10.1063/1.4774078

Min Y, Zhang K, Chen Y, Zhang Y (2012) Sonodegradation and photodegradation of methyl orange by InVO4/TiO2 nanojunction composites under ultrasonic and visible light irradiation. Ultrason Sonochem 19:883–889. https://doi.org/10.1016/j.ultsonch.2011.12.015

Miretzky P, Cirelli AF (2009) Hg (II) removal from water by chitosan and chitosan derivatives: a review. J Hazard Mater 167:10–23. https://doi.org/10.1016/j.jhazmat.2009.01.060

Monkhorst HJ, Pack JD (1976) Special points for Brillouin-zone integrations. Phys Rev B 13:5188. https://doi.org/10.1103/PhysRevB.13.5188

Pei Z, Ding L, Lin H, Weng S, Zheng Z, Hou Y, Liu P (2013) Facile synthesis of defect-mediated TiO 2–x with enhanced visible light photocatalytic activity. J Mater Chem a 1:10099–10102. https://doi.org/10.1039/C3TA12062G

Perdew JP, Burke K, Ernzerhof M (1996) Generalized gradient approximation made simple. Phys Rev Lett 77:3865. https://doi.org/10.1103/PhysRevLett.77.3865

Pfrommer BG, Côté M, Louie SG, Cohen ML (1997) Relaxation of crystals with the quasi-Newton method. J Comput Phys 131:233–240. https://doi.org/10.1006/jcph.1996.5612

Rai HS, Bhattacharyya MS, Singh J, Bansal TK, Vats P, Banerjee UC (2005) Removal of dyes from the effluent of textile and dyestuff manufacturing industry: a review of emerging techniques with reference to biological treatment. Crit Rev Environ Sci Technol 35:219–238. https://doi.org/10.1080/10643380590917932

Sakthivel S, Neppolian B, Shankar MV, Arabindoo B, Palanichamy M, Murugesan V (2003) Solar photocatalytic degradation of azo dye: comparison of photocatalytic efficiency of ZnO and TiO2. Sol Energy Mater Sol Cells 77:65–82. https://doi.org/10.1016/S0927-0248(02)00255-6

Samanta M, Mukherjee M, Ghorai UK, Sarkar S, Bose C, Chattopadhyay KK (2018) Ultrasound assisted catalytic degradation of textile dye under the presence of reduced graphene oxide enveloped copper phthalocyanine nanotube. Appl Surf Sci 449:113–121. https://doi.org/10.1016/j.apsusc.2018.01.118

Segall MD, Lindan PJ, Probert MA, Pickard CJ, Hasnip PJ, Clark SJ, Payne MC (2002) First-principles simulation: ideas, illustrations and the CASTEP code. J Condens Matter Phys 14:2717

Sharma M, Jain T, Singh S, Pandey OP (2012) Photocatalytic degradation of organic dyes under UV–visible light using capped ZnS nanoparticles. Sol Energy 86:626–633. https://doi.org/10.1016/j.solener.2011.11.006

Vanderbilt D (1990) Soft self-consistent pseudopotentials in a generalized eigenvalue formalism. Phys Rev B 41:7892. https://doi.org/10.1103/PhysRevB.41.7892

Vieira Y, Leichtweis J, Foletto EL, Silvestri S (2020) Reactive oxygen species-induced heterogeneous photocatalytic degradation of organic pollutant rhodamine B by copper and zinc aluminate spinels. J Chem Technol Biotechnol 95:791–797. https://doi.org/10.1002/jctb.6267

Wang J, Wang Z, Huang B, Ma Y, Liu Y, Qin X, Dai Y (2012) Oxygen vacancy induced band-gap narrowing and enhanced visible light photocatalytic activity of ZnO. ACS Appl Mater Interfaces 4:4024–4030. https://doi.org/10.1021/am300835p

Wang G, Huang B, Li Z, Lou Z, Wang Z, Dai Y, Whangbo MH (2015) Synthesis and characterization of ZnS with controlled amount of S vacancies for photocatalytic H 2 production under visible light. Sci Rep 5:1–7. https://doi.org/10.1038/srep08544

Wu T, Liu G, Zhao J, Hidaka H, Serpone N (1998) Photoassisted degradation of dye pollutants. V. Self-photosensitized oxidative transformation of rhodamine B under visible light irradiation in aqueous TiO2 dispersions. J Phys Chem B 102:5845–5851. https://doi.org/10.1021/jp980922c

Wu H, Zheng Z, Tang Y, Huang NM, Amal R, Lim HN, Ng YH (2018) Pulsed electrodeposition of CdS on ZnO nanorods for highly sensitive photoelectrochemical sensing of copper (II) ions. SUSTAIN MATER TECHNO 18:e00075. https://doi.org/10.1016/j.susmat.2018.e00075

Wu H, Tan TH, Liu R, Hsu HY, Ng YH (2020a) Selective ethanol oxidation to acetaldehyde on nanostructured zeolitic imidazolate framework-8-wrapped zno photothermocatalyst thin films. Sol.RRL 2000423. https://doi.org/10.1002/solr.202000423

Wu H, Zheng Z, Toe CY, Wen X, Hart JN, Amal R, Ng YH (2020b) A pulse electrodeposited amorphous tunnel layer stabilises Cu 2 O for efficient photoelectrochemical water splitting under visible-light irradiation. J Mater Chem a 8:5638–5646. https://doi.org/10.1039/D0TA00629G

Zhang J, Xu Q, Feng Z, Li M, Li C (2008a) Importance of the relationship between surface phases and photocatalytic activity of TiO2. Angew Chem Int 120:1790–1793. https://doi.org/10.1002/ange.200704788

Zhang W, Zhong Z, Wang Y, Xu R (2008b) Doped solid solution:(Zn0. 95Cu0. 05) 1–x Cd x S nanocrystals with high activity for H2 evolution from aqueous solutions under visible light. J Phys Chem C 112:17635–17642. https://doi.org/10.1021/jp8059008

Zhang X, Jia X, Duan P, Xia R, Zhang N, Cheng B, Zhang Y et al (2021) V2O5/Pg-C3N4 Z-scheme enhanced heterogeneous photocatalytic removal of methyl orange from water under visible light irradiation. Colloids Surf

608:125580. https://doi.org/10.1016/j.colsurfa.2020.125580

Zhou M, Yang H, Xian T, Li RS, Zhang HM, Wang XX (2015) Sonocatalytic degradation of RhB over LuFeO3 particles under ultrasonic irradiation. J Hazard Mater 289:149–157. https://doi.org/10.1016/j.jhazmat.2015.02.054